Inorg. Chem. **2003**, *42*, 5707–5714

Molecular QCA Cells. 1. Structure and Functionalization of an Unsymmetrical Dinuclear Mixed-Valence Complex for Surface Binding

Zhaohui Li, Alicia M. Beatty, and Thomas P. Fehlner*

Department of Chemistry and Biochemistry, University of Notre Dame, Notre Dame, Indiana 46556

Received December 11, 2002

Utilization of binary information encoded in the charge configuration of quantum-dot cells (the quantum-dot cellular automata, QCA, paradigm) requires molecule-sized dots for room temperature operation. Molecular QCA cells are mixed-valence complexes, and the evaluation and functionalization of an unsymmetrical heterobinuclear, two-dot, Fe–Ru molecular QCA cell is described. The solid state structures of *trans*-RuCl(dppm)$_2$(C≡CFc) (**1**) (dppm = methylbis(diphenylphosphane), Fc = (η^5-C_5H_5)Fe(η^5-C_5H_4)) and mixed-valence [*trans*-RuCl(dppm)$_2$(C≡CFc)][BF_4] (**1a**) as well as XPS and spectroscopic data suggest class II behavior suitable for the intended application. Utilization of the trans-Cl position of **1** permits functionalization for surface binding. Two "tailed" complexes of **1**, *trans*-Ru(dppm)$_2$(C≡CFc)(C≡CPhOCH$_3$) (**2**) and *trans*-[Ru(dppm)$_2$(C≡CFc)(N≡CCH$_2$CH$_2$NH$_2$)][PF_6] (**3**), have been prepared and characterized. The solid state structure of **3** and multinuclear NMR experiments define the structures. In addition, the spectroscopic properties of all complexes and their mixed-valence species are used to define the effect of the substituent "tail" on mixed-valence properties. Further, the electrochemistry of these compounds permits assessment of the extent of perturbation of the substituents on the comproportionation constants and overall electrochemical stability. The complexes possess properties necessary for candidate QCA molecules.

Introduction

Quantum-dot cellular automata (QCA), a new architecture for computation, are based on encoding binary information in the charge configuration of quantum-dot cells.[1−3] An ideal QCA cell consists of four quantum dots positioned at the corners of a square or two double-dot cells arranged side by side. Tunneling of two extra mobile electrons between neighboring sites of the cell constitutes switching between the two degenerate states. The interaction between QCA cells is sufficient to enable general purpose computing. QCA has now been demonstrated in micron-sized metal cells, wires, and majority gates.[4] Switching of a single electron in a double-dot cell can control the position of a single electron in another double-dot cell.[5] However these metal dot tunnel junction cells only operate at 80 mK as state energy differences are very small. As sizes of dots and junctions shrink, state energy differences and operating temperatures increase. Molecular scales (∼2 nm) are required for room temperature QCA operation.[6] Molecular-sized QCA cells are mixed-valence complexes, and the chemical properties of mixed-valence complexes have been well studied.[7,8]

However, not all mixed-valence compounds are suitable for QCA application. A two-dot QCA molecule must have (1) a stable mixed-valence state with a comproportionation constant of at least 10^3; (2) strong coupling between the redox centers (to permit rapid exchange of the charge between the two sites); (3) capability of functionalization for surface binding in ordered arrays; (4) a good preparative route from readily accessible starting materials; and (5) kinetic stability relative to degradation reactions. Although symmetrical cells are needed for "wires" and logic elements, an unsymmetrical two-dot cell with states of unequal stability constitutes a useful tool for testing whether mixed-valence complexes possess additional fundamental properties necessary for the QCA application.

* Author to whom correspondence should be addressed. E-mail: Fehlner.1@nd.edu.

(1) Lent, C. S.; Tougaw, P. D.; Porod, W.; Beinstein, G. H. *Nanotechnology* **1993**, *4*, 49.
(2) Lent, C. S.; Tougaw, P. D. *J. Appl. Phys.* **1993**, *74*, 6227.
(3) Lent, C. S. *Science* **2000**, *288*, 1597.
(4) Lent, C. S.; Tougaw, P. D. *Proc. IEEE* **1997**, *85*, 541.
(5) Fulton, T. A.; Dolan, G. H. *Phys. Rev. Lett.* **1987**, *59*, 109.
(6) Lent, C. S.; Tougaw, P. D.; Porod, W. *Proc. Workshop on Physics and Computing*; IEEE Computer Society Press: NY, 1994; pp 5−13.
(7) Creutz, C. *Prog. Inorg. Chem.* **1983**, *30*, 1.
(8) Kaim, W.; Klein, A.; Glockle, M. *Acc. Chem. Res.* **2000**, *33*, 755.

10.1021/ic026254y CCC: $25.00
Published on Web 08/14/2003

Recently complexes containing ferrocene, especially heterobimetallic complexes, have attracted attention for applications in the area of material science.[9−12] The Fe(II) center in ferrocene is an ideal redox center. Indeed, the Fe(II)/Fe(III) couple serves as a common reference in electrochemistry. The introduction of another transition metal in close proximity to the metallocene via a conjugating linker provides architectural flexibility and the fine-tuning of properties required for our application. *trans*-$RuCl(dppm)_2(C{\equiv}CFc)$, **1**, dppm = methylbis(diphenylphosphane), Fc = $(\eta^5\text{-}C_5H_5)Fe(\eta^5\text{-}C_5H_4)$, is a hetero-bimetallic, unsymmetrical Ru−Fc complex which was first reported by Colbert et al.[13,14] This complex displays two redox couples in its cyclic voltammogram (CV). However, the facts that the assignment of the two CV waves changed between the first and second publications, the solid state structures of neutral complexes, monocations, and dications are not known, and the molecule, as is, is not functionalized for surface binding led us to revisit the system.

In this study, we have reproduced the preparation of **1** and determined the solid state structures of the neutral and monocation (mixed-valence) complexes. We have also synthesized *trans*-$Ru(dppm)_2(C{\equiv}CFc)(C{\equiv}CPhOCH_3)$ (**2**) and [*trans*-$Ru(dppm)_2(C{\equiv}CFc)(N{\equiv}CCH_2CH_2NH_2)][PF_6]$ (**3**) which are suitable for binding to surfaces. The structures, spectroscopic properties, and electrochemistry of these complexes and their mixed-valence species are reported in order to evaluate the extent of perturbation of the surface binding tail of the complex on mixed-valence properties. The following paper[39] reports surface attachment and surface electrochemistry of **3** and its chemical conversion into a surface-bound, mixed-valence complex for ultimate use in QCA devices.

Experimental Section

General. Syntheses were carried out under dry argon using standard Schlenk methods. All procedures were carried out in the dark as much as possible (flasks and NMR tubes were wrapped in aluminum foil). All solvents were distilled prior to use. $FcC{\equiv}CH$ and *cis*-$RuCl_2(dppm)_2$ were synthesized following the methods reported in the literature.[15,16] $NaPF_6$, DBU (1,8-diazabicyclo[5.4.0]-undec-7-ene), and $HC{\equiv}CPhOCH_3$ were purchased from Aldrich and were used as received. Visible spectra were recorded on a Beckman DU-7500 spectrophotometer. NIR spectra were recorded on Thermo Nicolet Nexus 670 FT-IR spectrometer. IR spectra were recorded on a Perkin-Elmer Paragon 1000 FT-IR spectrometer, and samples were prepared as KBr pellets. NMR spectra were measured on a Varian 300 MHz instrument. Mass spectra (FAB^+) were recorded on a JEOL JMS-AX505HA mass spectrometer from a matrix of *p*-nitrobenzyl alcohol. Elemental analyses were conducted in the M-H-W Laboratories. Cyclic voltammetric measurements were performed on a BAS Epsilon-EC using a Pt working electrode, Pt-plate counter electrode, and Pt-wire pseudo-reference electrode. Tetrabutylammonium tetrafluoroborate ($TBABF_4$) (0.1 M) was used as the supporting electrolyte. All measurements are referenced to ferrocene. X-ray photoelectron spectroscopy (XPS) was carried out using a Kratos Analytical ESCA system with Mg Kα radiation at 1253.6 eV. The takeoff angle was fixed at 90°. Powder samples were mounted on sample stubs with conductive carbon tape. The binding energies for each peak were referenced to the C 1s peak at 284.6 eV.

***trans*-$RuCl(dppm)_2(C{\equiv}CFc)$ (1).** Following the literature method, to a stirred solution of $FcC{\equiv}CH$ (0.10 g, 0.48 mmol) in CH_2Cl_2 (30 mL) were added *cis*-$RuCl_2(dppm)_2$ (0.452 g, 0.48 mmol) and $NaPF_6$ (0.232 g, 0.6 mmol). After 4 h, the resultant red-brown solution was filtered. DBU (80 ηL) was added, and the red-brown solution changed immediately to orange. After it was stirred at room temperature for another 2 h, the reaction mixture was dried under vacuum. The resulting red-brown solid was dissolved in a minimum of CH_2Cl_2 and run through a column charged with Al_2O_3. The product was eluted with ether. Removal of the solvent yielded an orange solid. Recrystallization from CH_2Cl_2/ether gave orange crystals suitable for X-ray diffraction (0.165 g, 32%). IR (cm^{-1}): 2074 (C≡C). ^{31}P ($CDCl_3$): −5.03 (s). ^1H ($CDCl_3$): 7.1−7.6 (m, 40 H, Ph), 4.8−5.0 (m, 4H, CH_2P), 3.76 (t, 2H, C_5H_4), 3.66 (s, 5H, C_5H_5), 3.40 (t, 2H, C_5H_4).

***trans*-$[RuCl(dppm)_2(C{\equiv}CFc)][BF_4]$ (1a).** $[FcH][BF_4]$ (28 mg, 0.1 mmol) was added to $RuCl(dppm)_2(C{\equiv}CFc)$ (0.112 g, 0.1 mmol) in 20 mL of CH_2Cl_2, which resulted in an immediate color change from orange to blue. The reaction mixture was stirred at room temperature for 2 h, and then the solution was dried under vacuum to give a purple solid. The purple solid obtained was washed with 10 mL of ether three times and dried in a vacuum. Needle purple crystals suitable for X-ray analysis were obtained by crystallization from CH_2Cl_2/hexane (0.092 g, 78%). IR (KBr): 1998 cm^{-1} (C≡C). FAB^+ (nitrobenzyl alcohol matrix) *m*/*z*: 1114 ($[M - BF_4]^+$), 905 ($[M - BF_4 - (C{\equiv}CFc)]^+$), 869 ($[M - BF_4 - (C{\equiv}CFc) - Cl]^+$).

***trans*-$Ru(dppm)_2(C{\equiv}CFc)(C{\equiv}CPhOCH_3)$ (2).** $[RuCl(dppm)_2(C{\equiv}CFc)]$ (0.112 g, 0.1 mmol), $HC{\equiv}C(C_6H_4)OCH_3$ (20 μL), $NaPF_6$ (0.017 g, 0.11 mmol), and NEt_3 (40 μL) were stirred in CH_2Cl_2 (20 mL) for 12 h. The resultant brown solution was filtered, and DBU (20 μL) was added into it. The color changed from brown to orange immediately. The mixture was stirred for another 2 h and was dried under vacuum. The product was purified by running through a Al_2O_3 column using CH_2Cl_2/ether (2:1) as eluent. Golden needle crystals were obtained from CH_2Cl_2/ether (0.019 g, 15%). Anal. Calcd for $RuFeP_4OC_{71}H_{60}$: C, 70.41; H, 4.96. Found: C, 70.35; H, 5.02. IR (cm^{-1}): 2062 (C≡C). ^{31}P ($CDCl_3$): −2.5 (s) ^1H ($CDCl_3$): 7.0−7.8 (m, 40 H, Ph), 6.5 (d, 2H, PhO), 6.1 (d, 2H, PhO), 4.8−5.0 (m, 4H, CH_2P), 3.8 (t, 2H, C_5H_4), 3.74 (s, 3H, OCH_3), 3.70 (s, 5H, C_5H_5), 3.54 (t, 2H, C_5H_4). FAB^+ (nitrobenzyl alcohol matrix) *m*/*z*: 1201 ($[M]^+$), 1070 ($[M - (C{\equiv}CPhOCH_3)]^+$), 869 ($[M - (C{\equiv}CPhOCH_3) - (C{\equiv}CFc) - Cl]^+$).

***[trans*-$Ru(dppm)_2(C{\equiv}CFc)(N{\equiv}CCH_2CH_2NH_2)][PF_6]$ (3).** $[RuCl(dppm)_2(C{\equiv}CFc)]$ (0.060 g, 0.053 mmol) and $TlPF_6$ (0.02 gg, 0.058 mmol) were stirred in CH_2Cl_2 (10 mL), and $N{\equiv}CCH_2CH_2NH_2$ (40 μL, excess) was added. The resultant suspension was stirred in room temperature for 15 h. The resultant orange suspension was filtered,

(9) Kollmar, C.; Couty, M.; Kahn, O. *J. Am. Chem. Soc.* **1991**, *113*, 7994.
(10) Chi, K. M.; Calabrese, J. C.; Reiff, W. M.; Miller, J. S. *Organometallics* **1991**, *10*, 688.
(11) Butler, I. R. In *Organometallic Chemistry*; Abel, E. W., Ed.; Specialist Periodic Reports 21; Royal Society of Chemistry: London, 1992; p 338.
(12) Marder, S. R. *Inorganic Materials*; Bruce, D. W., O'Hare, D., Eds.; Wiley: Chichester, 1992; p 136.
(13) Colbert, M.; Ingham, S.; Lewis, J.; Long, N.; Raithby, P. *J. Chem. Soc., Dalton Trans.* **1994**, 2215.
(14) Colbert, M..; Lewis, J.; Long, N.; Raithby, P.; White, A.; Williams, D. *J. Chem. Soc., Dalton Trans.* **1997**, 99.
(15) Doisneau, G.; Balavoine, G.; Fillebeen-Khan. T. *J. Organomet. Chem.* **1992**, *425*, 113.
(16) Chaudret, B.; Commenges, G.; Poilblanc, R. *J. Chem. Soc., Dalton Trans.*, **1984**, 1635.

Scheme 1. Preparation of *trans*-Ru(dppm)$_2$(C≡CFc)(C≡CPhOCH$_3$) (**2**)

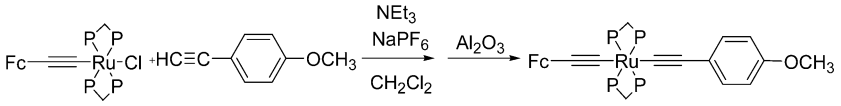

and the orange filtrate was dried under vacuum. The orange powder obtained was washed with ether and recrystallized from CH_2Cl_2/ether to give orange crystals suitable for X-ray diffraction (0.067 g, 95%). Anal. Calcd for $RuFeP_5F_6N_2C_{65}H_{59}$: C, 60.32; H, 4.56; N, 2.17. Found: C, 60.16; H, 4.57; N, 2.17. IR (cm^{-1}): 2089 (C≡C), 840 cm^{-1} (PF_6^-). ^{31}P ($CDCl_3$): −7.0 (s), −143 ppm (PF_6^-). ^{1}H ($CDCl_3$): 7.1−7.8 (m, 40 H, Ph), 4.8−5.2(m, 4H, CH_2P), 4.02 (s, 2H, C_5H_4), 3.91 (s, 2H, C_5H_4), 3.78 (s, 5H, C_5H_5), 1.91 (t, 2H, CH_2CH_2N), 1.53 (t, 2H, CH_2CH_2N). FAB$^+$ (nitrobenzyl alcohol matrix) *m*/*z*: 1149 ([M − PF_6]$^+$), 1079 ([M − PF_6 − (N≡CCH_2-CH_2NH_2)]$^+$), 869 ([M − PF_6 − (N≡$CCH_2CH_2NH_2$) − (HC≡CFc)]$^+$).

[*trans*-Ru(dppm)$_2$(C≡CFc)(N≡$CCH_2CH_2NH_2$)][PF_6][BF_4] (3a). [FcH][BF_4] (0.01 g, 0.037 mmol) and [Ru(dppm)$_2$(C≡CFc)(N≡$CCH_2CH_2NH_2$)][PF_6] (0.048 g, 0.037 mmol) were stirred in CH_2Cl_2 (10 mL). The color changed immediately from orange to red. After 2 h, the reaction mixture was dried under vacuum and washed with ether to give a red powder. Red needles were obtained by crystallization from CH_2Cl_2/hexane solution (0.040 g, 78%). IR (cm^{-1}): 2048 (C≡C), 838 cm^{-1} (PF_6^-).

Structure Determinations. Single crystals of **1**, **1a**, and **3** suitable for X-ray single-crystal diffraction were obtained by slow diffusion from CH_2Cl_2 to ether. Samples were placed in inert oil, mounted on a glass pin, and transferred to the cold gas stream of the diffractometer. Crystal data were collected and integrated using a Bruker Apex system, with graphite-monochromated Mo Kα (λ = 0.71073 Å) radiation at 100 K. The structures were solved by heavy atom methods using SHELXS-97 and refined using SHELXL-97 (Sheldrick, G. M., University of Göttingen). Non-hydrogen atoms were found by successive full matrix least squares refinement on F^2 and refined with anisotropic thermal parameters. Hydrogen atoms were placed at calculated positions, and a riding model with fixed thermal parameters [u_{ij} = 1.2U_{ij}(eq) for the atom to which they are bonded] was used for subsequent refinements.

Results and Discussion

Synthesis. The preparation of **2** follows the strategy reported for the preparation of *trans*-Ru(dppm)$_2$(C≡CFc)$_2$.[14] The substitution of chloride in **1** by a second acetylene ligand to give **2** was accomplished in the presence of NEt_3 (Scheme 1). Although crystals suitable for single-crystal X-ray diffraction could not be obtained, NMR and other spectroscopic data confirm its structure. Briefly, the four P atoms are equivalent and show only one signal at −2.5 ppm in the ^{31}P{^{1}H} NMR spectrum. The ^{1}H NMR shows three new signals. Two doublets at 6.5 and 6.1 ppm (1:1) can be assigned to the four protons of the phenyl ring in the tail while the single resonance at 3.74 ppm belongs to the OCH_3 group. A $\nu_{C\equiv C}$ band with a weak shoulder is observed in the IR spectrum at lower frequency (12 cm^{-1}) than for **1**, which also exhibits a weak shoulder. As **3** did not prove suitable for the intended application, the search for the presumably weak second band was not pursued.

Since the method used in preparing **2** involved tedious column separation and was of limited value for replacement

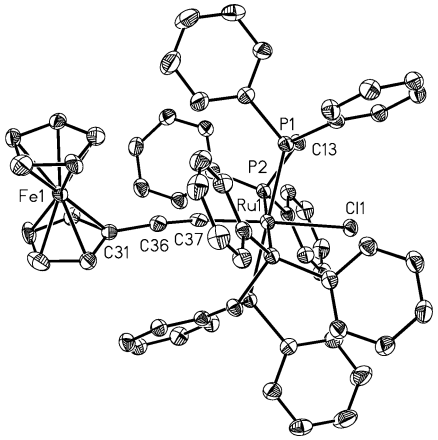

Figure 1. Molecular structure of *trans*-RuCl(dppm)$_2$(C≡CFc) (**1**) with 50% thermal ellipsoids (disordered atoms and hydrogen atoms not shown).

Scheme 2. Preparation of *trans*-[Ru(dppm)$_2$(C≡CFc)(N≡$CCH_2CH_2NH_2$)][PF_6] (**3**)

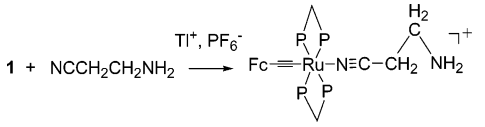

of chloride with other ligand types, a potentially more general method using $AgPF_6$ for Cl^- abstraction was employed in the preparation of **3**. Unfortunately, $AgPF_6$ preferentially oxidizes **1**. Hence, another Cl^- abstractor, $TlPF_6$, was tested. Reaction of **1** and $TlPF_6$ followed by addition of $NCCH_2$-CH_2NH_2 in situ gave a very complicated set of products from which nothing useful could be isolated. In contrast, a one-pot reaction using **1**, $TlPF_6$, and $NCCH_2CH_2NH_2$ gave an almost quantitative yield of **3** (Scheme 2).

The IR spectrum of **3** shows a single absorption at 2089 cm^{-1}. In contrast to **2** it appears at higher frequency than that of **1**. In addition to the expected signals from **1**, the ^{1}H NMR spectrum of **3** shows two triplets at 1.91 and 1.53 ppm which can be assigned to the two CH_2 groups of $NCCH_2$-CH_2NH_2. Compared to free $NCCH_2CH_2NH_2$, a substantial shift (∼1 ppm) to high field is observed for the two CH_2 resonances. This large high-field shift of the two CH_2 groups is due to shielding by the ring current of the Ph groups in the dppm ligands. These two CH_2 groups display a second-order AA′BB′ spin pattern in the ^{1}H NMR. No signals are observed for the two protons from NH_2 presumably because of rapid relaxation caused by an asymmetric electronic environment.

Solid State Structures. The structures of **1**, **1a**, and **3** are given in Figures 1−3, respectively. Some important bond lengths and bond angles of **1**, **1a**, and **3** are listed in Table 1, and the crystallographic data are summarized in Table 2. The structure of **1** is similar to its Os analogue.[13] The Ru atom lies on the crystallographic center of symmetry with the Cl and C≡C(C_5H_4)Fe(C_5H_5) units disordered about it, each with 50% occupancy. The Ru atom has distorted

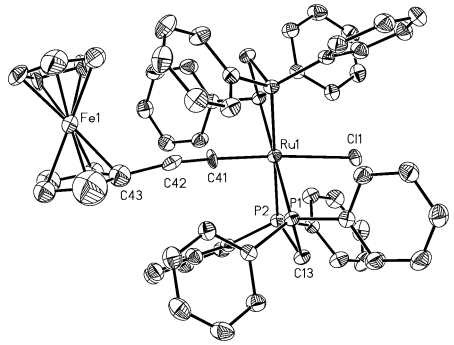

Figure 2. Structure of the cation of [*trans*-RuCl(dppm)$_2$(C≡CFc)][BF$_4$] (**1a**) with 50% thermal ellipsoids (disordered atoms and hydrogen atoms not shown).

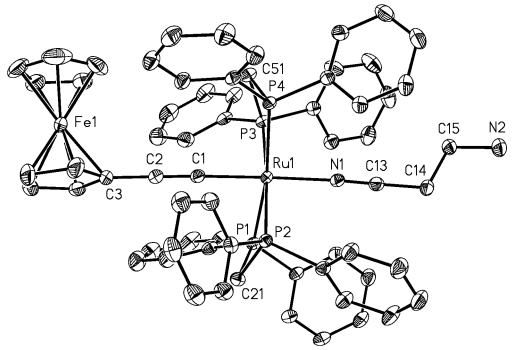

Figure 3. Structure of the cation of [*trans*-Ru(dppm)$_2$(C≡CFc)(N≡CCH$_2$CH$_2$NH$_2$)][PF$_6$] (**3**) with 50% thermal ellipsoids (hydrogens omitted).

octahedral coordination geometry. The Ru−C≡C−C$_5$H$_4$ bond angles are nearly linear, and the Ru−P distances (av 2.340(1) Å) fall in the normal range. The Ru−C(37) distance (2.019(9) Å) is comparable to that in complexes where Ru is σ bonded to ethynylic functions (e.g., 2.02(1) Å in (η^5-C$_5$H$_5$)(PPh$_3$)$_2$Ru(CCC(OCOCF$_3$)CMe$_2$,[17] 2.016(3) Å in (η^5-C$_5$H$_5$)(PPh$_3$)$_2$RuCCPh,[18] and 2.017(9) Å in (η^5-C$_5$H$_5$)(PPh$_3$)$_2$-Ru(CCPh·CuCl)[19]), but it is a little shorter than the Ru−C distance found in a bis(acetylide) ferrocene complex (Ru-(dppm)$_2${C≡C(C$_5$H$_4$)Fe(C$_5$H$_5$)}$_2$) (2.072(4) Å). The C(36)−C(37) distance (1.194(10) Å) falls in the normal range for C≡C bond lengths in metal acetylide complexes (1.18−1.24 Å).[20] The C(31)−C(36) distance (1.440(9) Å) corresponds to a single bond.

The Cl and C≡C(C$_5$H$_4$)Fe(C$_5$H$_5$) moieties in **1a** are also disordered about the Ru center, each with 50% occupancy as in **1**. In addition one of the cyclopentadienyl rings was found to be 2-fold disordered in **1a**. A larger deviation from linearity for C(41)−C(42)−C(43) (165.9(5)°), compared to **1**, is observed. The Ru−P distance (av 2.361(2) Å) is slightly longer than those found in the neutral **1** (av 2.340(1) Å). However, it is known that the Ru−P bond in cationic Ru complexes is slightly longer (by 0.02−0.04 Å) than that in neutral Ru complexes.[21,22] The Ru−Cl distance (2.436(2) Å) is slightly shorter than that in the neutral **1** (2.485(2) Å). The Ru−C(41) distance (1.876(9) Å) is shorter but comparable to some observed Ru=C distances (1.863 Å in [η^5-C$_5$H$_5$)(PPh$_3$)$_2$Ru(CCMePh)][PF$_6$][23] and 1.884 Å in [η^5-C$_5$H$_5$)(PMe$_3$)$_2$Ru(CCCPh$_2$)][PF$_6$]).[24] Not much change is observed in the C≡C distance (C(41)−C(42) (1.196(9) Å). The C(43A)−C(42) (1.518(3) Å) and C(43)−C(42) (1.602-(7) Å) distances are longer than that in **1** (C(31)−C(36), 1.440(9) Å); however, the significance of the difference is questionable considering the disorder of the Cp ring. While the observed structural differences do not allow definitive assignment of hole location, they might be used to support Ru(III) in the solid state.[25] However, the definitive X-ray photoelectron spectroscopic (XPS) experiments (see below) support hole localization at Fe, not Ru. Localization at Fe is confirmed by the solution electrochemical experiments.

In terms of geometric structure, the substitution of Cl of **1** by a nitrile group in going to **3** results in little change despite the positive charge. The distances Ru(1)−C(1) (2.023(2) Å), Ru(1)−P (av 2.360(4) Å), C(2)−C(3) (1.433-(2) Å), and C(1)−C(2) (1.217(2) Å) are comparable to those

Table 1. Selected Bond Lengths and Bond Angles for *trans*-RuCl(dppm)$_2$(C≡CFc) (**1**), [*trans*-RuCl(dppm)$_2$(C≡CFc)] [BF$_4$] (**1a**), and [*trans*-Ru(dppm)$_2$(C≡CFc)(N≡CCH$_2$CH$_2$NH$_2$)][PF$_6$] (**3**)

(1) RuCl(dppm)$_2$(C≡CFc) (**1**)

Ru(1)−C(37)	2.019(9)	Ru(1)−P(2)	2.335(1)
Ru(1)−P(1)	2.344(1)	Ru(1)−Cl(1)	2.485(2)
C(31)−C(36)	1.440(9)	C(36)−C(37)	1.194(10)
Fe(1)−C(31)	2.073(9)	Fe(1)−C(41)	2.044(9)
Fe(1)−C(34)	2.016(11)	Fe(1)−C(33)	2.023(8)
Fe(1)−C(45)	2.030(10)	Fe(1)−C(43)	2.030(12)
Fe(1)−C(32)	2.036(11)	Fe(1)−C(42)	2.040(7)
Fe(1)−C(35)	2.043(7)	Fe(1)−C(44)	2.052(9)
Fe(1)−Cp(1)	1.6441	Fe(1)−Cp(2)	1.6474
C(37)−Ru(1)−P(2)	94.2(3)	C(37)−Ru(1)−P(1)	100.9(3)
C(37)−Ru(1)−Cl(1)	177.0(4)	P(2)−Ru(1)−Cl(1)	84.97(7)
P(1)−Ru(1)−Cl(1)	81.56(7)	C(37)−C(36)−C(31)	175.3(7)
C(36)−C(37)−Ru(1)	172.2(9)		

(2) [RuCl(dppm)$_2$(C≡CFc)][BF$_4$] (**1a**)

Ru(1)−C(41)	1.876(9)	Ru(1)−P(2)	2.357(1)
Ru(1)−P(1)	2.365(1)	Ru(1)−Cl(1)	2.436(2)
C(43A)−C(42)	1.518(3)	C(41)−C(42)	1.196(9)
C(43)−C(42)	1.602(7)		
Fe(1)−Cp(1)	1.7522	Fe(1)−Cp(1A)	1.6948
Fe(1)−Cp(2)	1.6796		
C(41)−Ru(1)−P(2)	94.4(3)	C(41)−Ru(1)−P(1)	94.7(3)
C(41)−Ru(1)−Cl(1)	176.3(3)	P(2)−Ru(1)−Cl(1)	82.67(6)
P(1)−Ru(1)−Cl(1)	82.29(5)	C(41)−C(42)−C(43)	165.9(5)
C(42)−C(41)−Ru(1)	176.7(8)		

(3) [Ru(dppm)$_2$(C≡CFc)(N≡CCH$_2$CH$_2$NH$_2$)][PF$_6$] (**3**)

Ru(1)−C(1)	2.023 (2)	Ru(1)−N(1)	2.075(2)
[Ru(1)−P] av	2.360(4)	C(1)−C(2)	1.217(2)
C(2)−C(3)	1.433(2)	N(1)−C(13)	1.146(2)
N(2)−C(15)	1.453(2)	C(13)−C(14)	1.466(2)
C(14)−C(15)	1.542(2)		
C(1)−Ru(1)−N(1)	174.32(5)	C(2)−C(1)−Ru(1)	177.66(14)
C(13)−N(1)−Ru(1)	171.69(12)	C(1)−C(2)−C(3)	179.17(18)
N(1)−C(13)−C(14)	178.79(17)		

(17) Lomprey, J. R.; Selegue, J. P. *Organometallics* **1993**, *12*, 616.
(18) Wisner, J. M.; Bartczak, T. J.; Ibers, J. A. *Inorg. Chim. Acta* **1985**, *100*, 115.
(19) Raghavan, N. V.; Davis, R. E. *J. Cryst. Mol. Struct.* **1976**, *6*, 73.
(20) Nast, R. *Coord. Chem. Rev.* **1982**, *47*, 89.
(21) Bruce, M. I.; Wong, F. S.; Skelton, B. W.; White, A. H. *J. Chem. Soc., Dalton Trans.* **1982**, 2203.
(22) Consiglio, G.; Morandini, F.; Sironi, A. *J. Organomet. Chem.* **1986**, *306*, C45. Consiglio, G.; Morandini, F.; Ciani, G. F.; Sironi, A. *Organometallics* **1986**, *5*, 1976.
(23) Bruce, M. I. *Pure Appl. Chem.* **1986**, *58*, 553.
(24) Selegue, J. P. *Organometallics* **1982**, *1*, 217.
(25) Robin, M. B.; Day, P. *Adv. Inorg. Chem. Radiochem.* **1967**, *10*, 247.

Table 2. Crystallographic Data for *trans*-RuCl(dppm)$_2$(C≡CFc) (**1**), [*trans*-RuCl(dppm)$_2$(C≡CFc)] [BF_4] (**1a**), and [*trans*-Ru(dppm)$_2$(C≡CFc)(N≡$CCH_2CH_2NH_2$)][PF_6] (**3**)

	1	**1a**	**3**
chemical formula	$C_{62}H_{53}ClFeP_4Ru$	$C_{62}H_{53}BClF_4FeP_4Ru$	$C_{67}H_{64}Cl_1F_6FeN_2O_{0.5}P_5Ru$
fw	1114.29	1201.10	1374.30
λ (Å)	0.71073	0.71073	0.71073
T (K)	100	100	100
space group	$P\bar{1}$	$C2/c$	$P\bar{1}$
a (Å)	10.0782(5)	21.8721(10)	11.2685(4)
b (Å)	12.2991(7)	18.9451(8)	13.7950(5)
c (Å)	12.5576(7)	13.1305(6)	21.1869(8)
α (deg)	118.1750(10)	−90	−102.4060(10)
β (deg)	109.1280(10)	−90.3350(10)	−103.5270(10)
γ (deg)	90.8880(10)	−90	−91.5190(10)
V (Å^3)	1268.99(12)	5417.4(4)	3117.1(2)
Z	1	4	2
R1,[a] wR2[b] ($I > 2\sigma(I)$)	R1 = 0.0379, wR2 = 0.0909	R1 = 0.0607, wR2 = 0.01430	R1 = 0.0344, wR2 = 0.0883
R1,[a] wR2[b] (all data)	R1 = 0.0389, wR2 = 0.0913	R1 = 0.0633, wR2 = 0.01439	R1 = 0.0388, wR2 = 0.0914

[a] $R1 = \sum||F_o| - |F_c||/\sum|F_o|$. [b] $wR2 = \{\sum\omega|[(F_o^2 - F_c^2)^2]/\sum\omega F_o^4\}^{1/2}$; $\rho = [(F_o^2,\theta) + 2F_c^2]/3$.

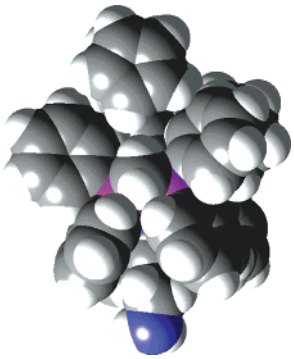

Figure 4. Space-filling model of [*trans*-Ru(dppm)$_2$(C≡CFc)(N≡$CCH_2CH_2NH_2$)][PF_6] (**3**) with the NH_2 tail at the bottom and Fc at the top.

found in **1**. The N≡C fragment coordinates linearly to the Ru atom (C(1)−Ru(1)−N(1), 174.32(5)°, C(13)−N(1)−Ru(1), 171.69(12)°, and N(1)−C(13)−C(14), 178.79(17)°). The distances Ru−N(1) (2.075(2) Å) and N≡C (1.146(2) Å) are comparable to those found in *cis*-[Ru(dppm)$_2$Cl(NCCH_3)][PF_6] (Ru−N 2.082 Å; N≡C 1.131 Å).[26] At the level of geometry, then, the substitution of Cl^- by an electron-withdrawing RCN ligand involved in attaching the tail has no effect. As discussed below, this substitution does perturb other properties. The two CH_2 groups of the NCCH_2-CH_2NH_2 tail lie in the shielding field of the phenyl groups corroborating the interpretation of the NMR shifts. The space-filling diagram (Figure 4) shows the NH_2 surface binding group protruding just far enough out of the "thicket" of Ph groups of **1** to allow it to be used for surface attachment. This short tail is designed to minimize deviations of the surface-bound complex from a vertical orientation. Figure 5 shows the anion−cation packing in a crystal of **3**. The $[PF_6]^-$ anions lie considerably closer to the Fe centers than the Ru centers (6.11 vs 8.57 Å) in the solid state. Possibly the bulky dppm ligands of the Ru center are the cause.

Spectroscopic Properties. Chemical oxidation of **1** with [FcH][BF_4] led to nearly quantitative formation of the mixed-valence **1a** as an air-stable purple powder. The IR spectrum of **1a** shows a strong, broad absorption at 1998 cm^{-1} in

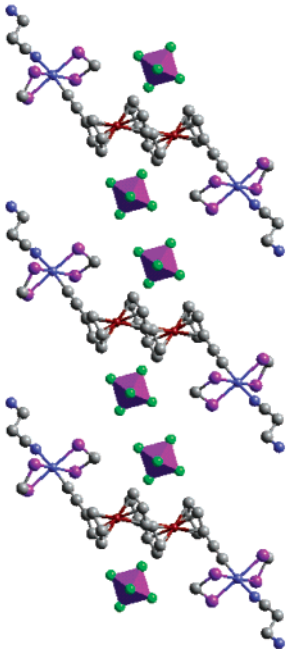

Figure 5. Packing diagram of Ru(dppm)$_2$(C≡CFc)(N≡$CCH_2CH_2NH_2$)]-[PF_6] (**3**) showing the location of the anions (octahedra) relative to Fe and Ru.

contrast to the weak, sharp absorption observed at 2074 cm^{-1} for neutral **1**. Shifting of $\nu_{C\equiv C}$ to lower frequency has been observed in some Fe(II) ferrocenylacetylide complexes [(Cp or Cp*)(PP)FeC≡CFc][27] and some bis(acetylide) ferrocene complexes. Recently, it was reported that the conversion of MC≡C−C≡CM to its one-electron-oxidized radical cation results in a shift of $\nu_{C\equiv C}$ to a value lying between the frequencies of the neutral and the doubly oxidized species due to rapid electron transfer (>10^{12} s^{-1}) in the system.[28,29] Hence, one interpretation of the broad peak and the ≈80 cm^{-1} shift to lower energy observed for **1a** is thermal electron transfer between the metal centers faster than the IR time scale (10^{12} s^{-1}). This requires that the broad absorption band

(26) Winter, R. F.; Scheiring, T. *Z. Anorg. Allg. Chem.* **2000**, *626*, 1196.
(27) Sato, M.; Hayashi Y.; Kumakura S.; Shimizu, N.; Katada M.; Kawata, S. *Organometallics* **1996**, *15*, 721.
(28) Seyler, J. W.; Weng, W.; Zhou, Y.; Gladysz, J. A. *Organometallics* **1993**, *12*, 3802.
(29) Le Narvor, N.; Lapinte, C. *J. Am. Chem. Soc.* **1995**, *117*, 7129.

Table 3. Electronic Absorption Energies and Related Data for [*trans*-RuCl(dppm)$_2$(C≡CFc)][BF_4] (**1a**)[a] and [*trans*-Ru(dppm)$_2$(C≡CFc)(N≡$CCH_2CH_2NH_2$)][PF_6][BF_4] (**3a**)

complex	UV (nm)	NIR (ν_{max}, cm^{-1})	$\Delta\nu_{1/2}$ (cm^{-1})	ϵ^b (M^{-1} cm^{-1})	$\Delta E_{1/2}$ (V)	$\nu_{0(calc)}$ (cm^{-1})	$\Delta\nu_{1/2(calc)}$ (cm^{-1})	$10^2\alpha^2$
1a	440, 590	6220, 4630	2200	3000	0.70	5600	1197	1.2
	438, 600	*6570*	*1982*		*0.70*	*5600*	*1496*	*0.31*
3a	405, 513	8480, 4350	2730	850	0.99	7920	1137	0.3

[a] Values in italics for **1a** are from ref 14. [b] Value for the highest energy IVCT band.

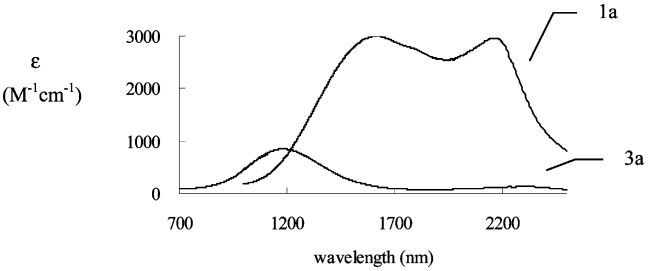

Figure 6. NIR spectrum of [*trans*-RuCl(dppm)$_2$(C≡CFc)][BF_4] (**1a**) and [*trans*-Ru(dppm)$_2$(C≡CFc)(N≡$CCH_2CH_2NH_2$)][PF_6][BF_4] (**3a**) in $CDCl_3$.

Scheme 3. Two Limiting Structures for [*trans*-RuCl(dppm)$_2$(C≡CFc)][BF_4] (**1a**)

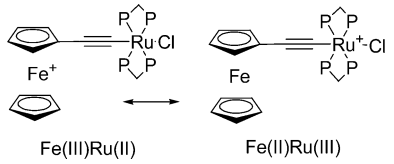

observed be the average of the two limiting species shown in Scheme 3 contributing to the structure of **1a**. The IR of the doubly oxidized species of **1** would have provided confirmation; however it could not be isolated.

However, the most likely explanation is that thermal electron transfer is slow and, because we deal with an unsymmetrical mixed-valence complex, the equilibrium population of the Fe(III)−Ru(II) species is substantially larger than that of the Fe(II)−Ru(III). This, coupled with the low dynamic range of the IR technique, leads to a single band. The shift to lower energy could well result from accommodation of the net charge on the complex, logically by back-donation from ruthenium, to generate some allenylidene character.

Complex **3a** is also prepared by reacting **3** with 1 molar equiv of [FcH][BF_4]. It is a deep red rather than purple color that shows that the electronic effects of Cl^- vs RCN are significant. Recrystallization from CH_2Cl_2/hexane gave deep red needle crystals. However attempts to grow crystals suitable for X-ray analysis were not successful. Like **1a**, a shift (2048 vs 2089 cm^{-1}) to lower frequency was observed for $\nu_{C\equiv C}$ in **3a**. However, in contrast to **1a**, it is sharper and the shift of smaller magnitude. Hence, we sought to compare the electronic properties of the mixed-valence complex with and without a tail.

Electronic absorption energies and related data for **1a** and **3a** are shown in Table 3. Figure 6 shows the near-infrared (NIR) spectra of **1a** and **3a**. Complex **1a** shows two broad absorptions at 1608 and 2160 nm in the NIR region. Two absorptions are also observed at similar positions for some mixed-valence (η^5-C_5H_5)L_2Ru(C≡C)Fc (L_2 = $2PPh_3$, dppe, or dppf).[30] Consistent with the literature, the absorption near 1600 nm is assigned to IVCT involving light-induced electron transfer between the dissimilar ferrocene and Ru centers. The assignment of the other absorption near 2200 nm is unclear. Complex **3a** also shows two peaks but at 1179 and 2298 nm. Compared with **1a**, the first peak in **3a** is at higher energy with a lower ϵ, while the second peak is at lower energy with an even lower ϵ. The large difference of the NIR absorption between **1a** and **3a** upon substitution at the Ru center can be taken as evidence of either hole localization at the Ru center or a strongly delocalized system.

The stabilization of a mixed-valence complex by solvation is said to be strongly dependent on the extent of electron delocalization in the system. The larger the interaction between the metals in the mixed-valence complex is, the smaller the influence of solvent on the IVCT band becomes. To empirically compare the mixed-valence properties of **1a** and **3a**, the effects on these absorptions of changing solvents from $CDCl_3$ to CD_3COCD_3 to CD_3CN to *d*-DMSO were examined. The NIR band maxima in these two complexes do not shift much as a function of solvent polarity (maximum shift of 35 nm for **1a** and 40 nm for **3a**). This indicates that the solvent reorganization associated with the electronic transition is small even though the dimetal mixed-valence complex is unsymmetrical.

To provide a more quantitative comparison, the spectroscopic data were processed with Hush theory. The parameters so generated are often used for intercomparison of mixed-valence complexes and provide an approximate measure of the nature of the electronic structure of a mixed-valence complex. The equation $\nu_{max} - \nu_0 = (\Delta\nu_{1/2})^2/2310$ (cm^{-1}),[14] where ν_0 is the internal energy difference between the two oxidation state isomers, permits $\Delta\nu_{1/2}$ to be calculated from ν_{max} provided ν_0 is estimated. An upper limit on ν_0 is provided the difference in the redox potentials of the two metal centers.[31] The ratio of $\Delta\nu_{1/2(obs)}$ and $\Delta\nu_{1/2(calc)}$ is often found to be considerably larger than 1 for class III systems. The calculated ratio $\Delta\nu_{1/2(obs)}/\Delta\nu_{1/2(calc)}$ is 1.8 and 2.4 for **1a** and **3a**, respectively. These are marginally higher than those observed for class II systems.

The equation $\alpha^2 = [(4.2 \times 10^{-4})\epsilon_{max}\Delta\nu_{1/2}]/\nu_{max}d^2$, where *d* is the distance between the metal centers, permits the calculation of a delocalization parameter, α^2, which has also been used in the past to classify mixed-valence systems. The distance between Fe and Ru is 6.128 Å in **1a** and 6.190 Å in **3** (assumed similar in **3a**) and is taken to represent *d*. Using

(30) Sato, M.; Shintate, H.; Kawata, Y.; Sekino, M.; Katada, M.; Kawata, S. *Organometallics* **1994**, *13*, 1956.
(31) Dowling, N.; Henry, P. M.; Lewis, N. A.; Taube, H. *Inorg. Chem.* **1981**, *20*, 2345.

Table 4. CV Data for *trans*-RuCl(dppm)$_2$(C≡CFc) (**1**), *trans*-Ru(dppm)$_2$(C≡CFc)(C≡CPhOCH$_3$) (**2**), and [*trans*-Ru(dppm)$_2$(C≡CFc)(N≡CCH$_2$CH$_2$NH$_2$)][PF$_6$] (**3**)[a]

complex	$E_{1/2}(1)$ (V)	$E_{pa}(1)$ (V)	$E_{pc}(1)$ (V)	$E_{1/2}(2)$ (V)	$E_{pa}(2)$ (V)	$E_{pc}(2)$ (V)	$\Delta E_{1/2}$[c] (V)	ref
1	−0.40	−0.34	−0.46	0.30	0.35	0.25	0.70	this work
1	−0.39			0.37			0.76	13
Fc(C≡C)(Os(dppm)$_2$Cl)	−0.44			0.21			0.65	13
2	−0.43	−0.38	−0.48	0.06	0.11	0.01	0.49	this work
3	−0.20	−0.15	−0.25	∼0.78[b]	0.86	0.70	∼0.98	this work

[a] Electrolyte 0.1 M [NBu$_4$][BF$_4$] in CH$_2$Cl$_2$; Pt electrode, 25 °C, scan rate 100 mV/s. $E_{1/2}$ values are referenced to ferrocene in the same system. [b] $E_{1/2}(2) = (1/2)[E_{pa}(2) + E_{pc}(2)]$ (irreversible for **3**). [c] $\Delta E_{1/2} = E_{1/2}(2) - E_{1/2}(1)$.

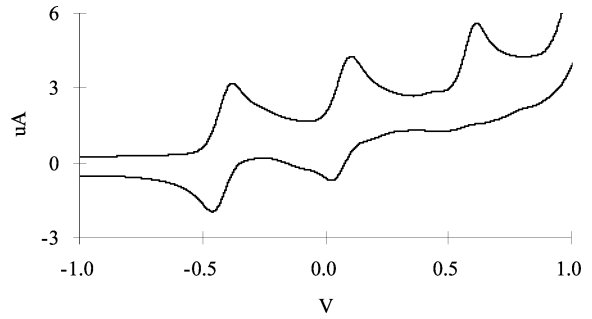

Figure 7. CV of *trans*-Ru(dppm)$_2$(C≡CFc)(C≡CPhOCH$_3$) (**2**) in CH$_2$Cl$_2$ (scan rate 100 mV/s, referenced to FcH/FcH$^+$).

the observed ϵ_{max}, $\Delta\nu_{1/2}$, and ν_{max}, the calculated α^2 for **1a** is 1.2×10^{-2}, which larger than that reported previously[14] as well as larger than typically observed for class II systems. However, the calculated α^2 for **3a** is 3×10^{-3}, which is comparable to some reported for class II systems. For example $\alpha^2 = 2.4 \times 10^{-3}$ in [FcC≡CFc]PF$_6$.[32]

The calculated parameters for **1a** and **3a** provide a measure of the effect of replacement of Cl$^-$ by RCN on the mixed-valence character of the complex. The latter ligand is expected to reduce the electron density on Ru via π metal to ligand back-donation. One suspects that the strength of the Ru−Fe interaction will decrease as the electron density on Ru decreases based on Sato's conclusion derived from a study of FcC≡CPt(PPh$_3$)$_2$(C$_6$H$_4$-X-*p*).[33] Most importantly, although the tailed ligand does change the mixed-valence character of the binuclear system, the change is not sufficiently large to obviate its use as a molecular QCA cell.

Electrochemistry. The electrochemical data for **1**, **2**, **3**, and the Os analogue of **1** are summarized in Table 4. The cyclic voltammograms (CVs) of **2** and **3** in CH$_2$Cl$_2$ containing 0.1 M [NBu$_4$][BF$_4$] are shown in Figures 7 and 8. The CV of **2** shows two quasi-reversible waves at −0.43 [$\Delta E_p(1) = 0.1$ V, $i_{pa}/i_{pc} \sim 1$] and 0.06 V [$\Delta E_p(2) = 0.1$ V, $i_{pa}/i_{pc} \sim 0.6$] (vs FcH/FcH$^+$). The oxidation wave at 0.57 V is attributed to the oxidation of the ligand −C≡CPhOCH$_3$. Complex **3** shows one quasi-reversible wave at −0.20 V [$\Delta E_p(1) = 0.1$ V, $i_{pa}/i_{pc} \sim 1$] and one irreversible wave $E_{pa}(2) = 0.86$ V and $E_{pc}(2) = 0.70$ V [$\Delta E_p(2) = 0.16$ V, $i_{pa}/i_{pc} \sim 0.5$] (vs FcH/FcH$^+$). An additional wave was observed at $E_{pc} = -1.38$ V (vs FcH/FcH$^+$) (Figure 8a). This wave did not appear when the scanning turned back at +0.2 V (Figure 8b) and reflects instability of the doubly oxidized species. The intensity of the reduction wave at 0.70 V decreased with repetitive cycling. But the intensity of the wave at −0.20 V did not change after several scans if the scanning reversed at 0.20 V. Fortunately, QCA use only requires access to the mixed-valence state and the chemical instability of the tailed, doubly oxidized complex need not be a problem.

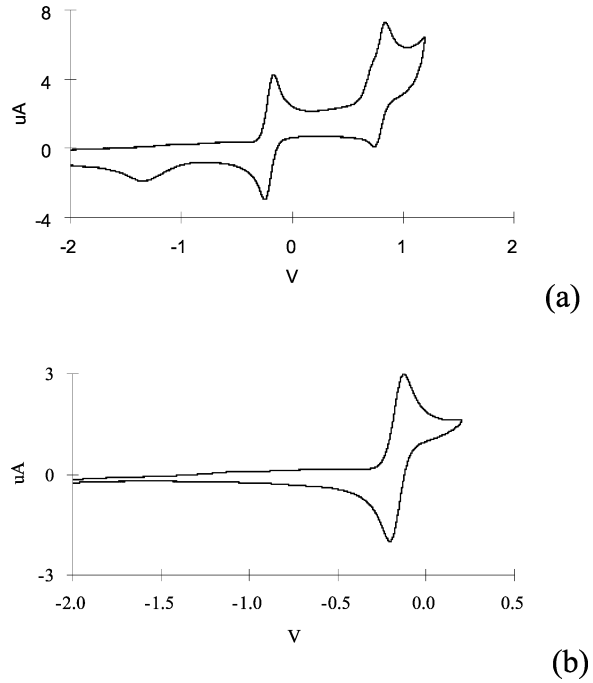

Figure 8. CV of [*trans*-Ru(dppm)$_2$(C≡CFc)(N≡CCH$_2$CH$_2$NH$_2$)][PF$_6$] (**3**) in CH$_2$Cl$_2$: (a) scan from −2.0 to 1.2 V (scan rate 100 mV/s, referenced to FcH/FcH$^+$); (b) scan from −1.8 to 0.2 V (scan rate 50 mV/s, referenced to FcH/FcH$^+$)

The CV data show that the redox potentials of these complexes are substantially influenced by ligand substitution at the Ru center. A comparison of the CVs of **1** and **2** shows that replacement of chloride in **1** by −C≡CPhOCH$_3$ results in a cathodic shift by 0.24 V in the second wave. However the first wave is nearly unaffected by the ligand substitution. The cathodic shift is attributed to a better electron-donating ability of −C≡CPhOCH$_3$ compared to chloride. Comparison of the CVs of **1** and **3** shows the 0.2 V anodic shift for the first redox wave expected for a cationic complex **3** compared to neutral **1**. Comparison of the second redox waves shows that the substitution of chloride by N≡CCH$_2$CH$_2$NH$_2$ causes an anodic shift by 0.48 V. The π back-donation from the Ru center to the N≡CCH$_2$CH$_2$NH$_2$ acceptor accounts for the anodic shift. The CV data of **1**, **2**, and **3** indicates that the substituent on the Ru center adjusts the electron density on the Ru atom but this substituent effect is not transferred through the acetylene bond to the ferrocenyl moiety.

(32) Powers, M. J.; Meyer, T. J. *J. Am. Chem. Soc.* **1978**, *100*, 4393.
(33) Sato, M.; Mogi, E.; Katada, M. *Organometallics* **1995**, *14*, 4837.

Results from the CV experiment suggest the assignment of the first wave to the oxidation of the Fc center and the second wave to the oxidation of Ru center. This is in agreement with the conclusion of Colbert et al. based on some similar heterobimetallic bis(acetylide) ferrocene complexes. Comparison of the CV of **1** and its Os analogue *trans*-Fc(C≡C)[Os(dppm)$_2$Cl] shows that the potential of the first wave is almost the same whereas a small cathodic shift is observed for the second wave in the Os analogue. This again suggests that the first oxidation in solution takes place at the Fc center and that substitution of Ru by Os does not change the redox properties of this system significantly.

The presence of two well-separated one-electron oxidations indicates significant stabilization of the mixed-valence species relative to comproportionation into the (II−II) and (III−III) species. Although the degree of metal−metal interaction affects the electrochemical behavior of these systems, $\Delta E_{1/2}$ is caused mainly by an inherent redox dissymmetry and to a lesser extent by the degree of metal−metal interaction. Hence, in these systems, $\Delta E_{1/2}$ alone is not a measure of the degree of metal−metal interaction.

The differences in the oxidation potential between the two metal centers in **1**, **2**, and **3** are 0.70, 0.49, and 0.98 V, respectively. It is known that the energy of the IVCT band is correlated to the oxidation potential difference in heterobimetallic complexes.[34] Comparing the ΔE of **1** and **3**, we find that the one with the smaller ΔE (0.70 V for **1**) also has the lower energy IVCT band (1608 nm). Complex **3** has a higher ΔE (0.98 V) and a high-energy IVCT band at 1197 nm. This phenomenon has also been reported for Cp(dppe)-FeC≡CFc and Cp(dmpe)FeC≡CFc. The difference in the oxidation potentials for the two Fe(II/III) couples of Cp-(dppe)FeC≡CFc (0.59 V) and Cp(dmpe)FeC≡CFc (0.80 V) correlates with the energy of the IVCT band. Mixed-valence [Cp(dppe)FeC≡CFc]$^+$ has an intense, broad IVCT band at 1590 nm, while [Cp(dmpe)FeC≡CFc]$^+$ has a band at 1295 nm.

X-ray Photoelectron Spectroscopy. Since the time associated with an XPS measurement is very small ($\sim 10^{-17}$ s), the metal ionization energies of powder samples of **1** and **1a** were measured and compared.[35] Both samples contained peaks corresponding to the expected elemental compositions. Referenced to carbon, the Ru 3P$_{1/2}$ and Ru 3P$_{3/2}$ binding energies are the same within experimental error. However, the Fe 2P$_{1/2}$ and Fe 2P$_{3/2}$ ionizations in the spectrum of **1a** shift significantly and equally to higher binding energy relative to the corresponding peaks in the spectrum of **1** (723.5, 710.7 eV in **1a** vs 721.7, 709.2 eV in **1**) referenced to C 1s = 284.6 eV. A similar higher binding energy shift in the Fe core ionizations observed in *trans*-Ru(dppm)$_2$(C≡CFc)$_2$ when it was oxidized has been attributed to the formation of Fe^{III} upon oxidation.[36] Hole localization on Fe in the solid state (class II behavior) is suggested fully consistent with the electrochemical assignments in solution.

Conclusions

The structures, spectroscopic properties, and electrochemistry of heterobimetallic Ru−Fe complexes provide clear definition of its properties relative to use for molecular QCA. Chemically stable mixed-valence states of these complexes (**1a** and **3a**) can be obtained. The combined structural, spectroscopic, and electrochemical data show that these complexes exhibit properties associated with biased class II mixed-valence. Functionalization of **1** with the surface-binding OCH_3 and NH_2 has been achieved without major change in the mixed-valence properties of the coupled Ru−Fe centers. Hence, complex **3** satisfies the fundamental requirements for a biased two-dot molecular QCA cell. Along with recent calculational results, the case for utilization of mixed-valence complexes for molecular QCA is promising.[37,38] The attachment and characterization of these molecules on the surface of a solid substrate are described in the following paper.[39]

Acknowledgment. We thank Dr. Bindu Varughese for assistance with the XPS experiments and Professors A. G. Lappin and M. Lieberman for helpful discussions. The constructive comments of the referees are appreciated. A grant from ONR/DARPA (N00014-00-1-0746) is gratefully acknowledged.

Supporting Information Available: X-ray crystallographic files in CIF format for the structure determinations of **1**, **1a**, and **3**. This material is available free of charge via the Internet at http://pubs.acs.org.

IC026254Y

(34) Zhu, Y.; Clot, O.; Wolf, M. O.; Yap, G. P. A. *J. Am. Chem. Soc.* **1998**, *120*, 1812.
(35) Citrin, P. H. *J. Am. Chem. Soc.* **1973**, *95*, 6472.
(36) Jones, N. D.; Wolf, M. O.; Giaquinta, D. M. *Organometallics* **1997**, *16*, 1352.
(37) Lent, C. S.; Isakaen, B.; Lieberman, M. *J. Am. Chem. Soc.* **2003**, *125*, 1056.
(38) Braun-Sand, S. B.; Wiest, O. *J. Phys. Chem. A* **2003**, *107*, 285.
(39) Li, Z.; Fehlner, T. P. *Inorg. Chem.* **2003**, *42*, 5715−5721.